periodica polytechnica

Mechanical Engineering
56/2 (2012) 117–124
doi: 10.3311/pp.me.2012-2.07
web: http://www.pp.bme.hu/me

RESEARCH ARTICLE

Thermal simulation of a pin on a rotating cylinder jacket system

Gábor Bódai / *Károly* Váradi / *János* Szücs / *András* Szabó / *István* Zobory

Received 2012-06-30

Abstract

In this paper specimen level measurements and finite element simulations are introduced in order to study the thermal behaviour of a pin and wheel sliding contact configuration. The pin-like specimen is processed from cast iron and models the local contact of a railway brake block and wheel tire. The sliding contact is treated in the framework of a 3 dimensional problem in order to achieve reliable results. The paper also treats with the heat partition problem by distributed heat source and moving heat source models. The results are compared to measured datas and show that the classical heat partition approach is not valid for the friction pair examined i.e. the contact. However authors determine the exact heat partition ratio by an iterative approach and give explanations on the experienced temperature differences.

Keywords

Railway braking · Frictional heat generation · heat partition · FE analyses

Acknowledgement

The work reported in the paper has been developed in the framework of the project "Talent care and cultivation in the scientific workshops of BME" project. This project is supported by the grant TÁMOP-4.2.2.B-10/1–2010-0009.

Gábor Bódai
Department of Machine and Product Design, BME, H-1111, Budapest, Műegyetem rkp. 3, Hungary
e-mail: bodai.gabor@gt3.bme.hu

Károly Váradi
János Szücs
Department of Machine and Product Design, BME, H-1111, Budapest, Műegyetem rkp. 3, Hungary

András Szabó
István Zobory
Department of Railway Vehicles and Vehicle System Analyses, BME, H-1111, Budapest, Műegyetem rkp. 3, Hungary

1 Introduction

In spite of the fact that the first appearance of railway technology dates back to the 16^{th} century, the intensive development has not stopped nowadays. Approaching the railway vehicles from the viewpoint of braking, frictional heat generation is an important central problem. As it is well-known the heat generated by friction -which evolves between two deformable solid bodies having nonzero sliding velocity on the contact spot- is able to drastically change the mechanical and wear behavior of the friction parts. It means that the deformation and stress state is strongly modified by the heat generation, which exerts significant influence also on type and value of wear. The momentary temperature rise of 50-500°C can result thermal stresses, changed material properties, unbalanced friction coefficients, severe wear and further thermal, frictional and dynamical instabilities. These effects and they connections generate an increasing research activity in the field of measurements [1–3] and especially in numerical modeling [4–6]. This paper focuses on a thermal problem, where the temperature rise has crucial consequences on the safe run. The mentioned frictional contact is characteristic between the wheel and the brake block and release on the large number of systems used in the railway industry. In the sizing of this part it is essential to take into consideration the long braking time, high brake block forces, which generally cause intensive wear and extreme high temperatures in the proximity of the contacting interfaces. This interrelation is thoroughly studied in the literature. In [7] Vernersson examines the braking process realizing between the brake block/wheel contact. He has found that the measured temperature changes, which starts the evaluation of hot spots on the wheel surface. They found correlation with the measured surface roughness. Vernersson in [8] gives the numerical explanation of the measured hot spots by contact and thermal finite element (FE) simulations and also give some results for the wear phenomena. However the final conclusions are not complete and the main conclusion of the work is the necessity of three dimensional models in the analysis.

The main motivation for this study is the desire to understand and simulate the thermal behavior of a pin on wheel configu-

ration representing the local behavior of a brake block / wheel sliding contact. The reasons why authors use pins instead of real braking block during the experimental and numerical examinations are the clear and transparent results. The temperature distributions and the heat partitions are identified by steady and transient calculations and authors prove that the heat partition varies during warming. The calculations also reveal that in a thermal system containing contacting partners with high rotation speed, the simple heat partition theory is not valid and cannot be used for precise estimation of the temperatures arising in the proximity of the contacting surfaces.

2 Experiments

The tests were performed at the Laboratory of Budapest Technical University and Economics (BUTE) at the Department of Railway Vehicles and Vehicle System Analysis. The picture of the testing rig can be seen in Fig. 1. The examined specimen (pin) was processed of a high phosphor content P14 cast iron brake block with the specimen length of 80 mm. The cross section of the specimen had nominal dimensions of 10×5 mm. The specimen connected to pre-prepared specimen holder (see Fig. 2 and Fig. 3) which in the fastening was realized by two screws. The material of the specimen holder was S235JR ISO standard steel. In the tests the pin was pushed against the jacket of a rotating wheel which had the diameter of 243 mm and width of 35 mm. The tangential and normal force components were measured by force sensors (2000 N MIKI with 2 mV/V cell parameter) while the temperature change was registered by thermo couples on the pin side and by laser technique on the rotating wheel side.

The applied angular velocity was 14.6 1/s, which is identical with the speed of 40.14 km/h (11.15 m/s). The nominal value of the applied constant normal load (100 N) was chosen in order to ensure the average contact pressure of 2 MPa. Considering the real structural level brake shoes this value corresponds with about 4000 N braking force which is representing average value in a general application.

The testing rig consists of an electric motor which drives the shaft of the wheel by a drive-belt. The shaft is directly connected to the wheel and is able to rotate it between 0 and 25 1/s angular velocity. The examined pin-like specimen can be pushed against the sliding cylindrical surface with the normal force of 0 and 2000 N adjusted by a hydraulic cylinder. The specimen holder is supported by two bearings and a suspension link system. The schematic illustration of the tested configuration can be seen in Fig. 2. In the figure just the sixth of the wheel is shown.

The main components of the specimen holder are depicted in Fig. 3. The orientation of the coordinate system is indicated in the figure in order to ensure full understanding compared to Fig. 2. The exploded view contains the locations where the temperature measurements were carried out by thermocouples. The 3^{rd} measured point -where the maximal temperature is expected- was located 3 mm till the end of the pin in the middle of the 10 mm width.

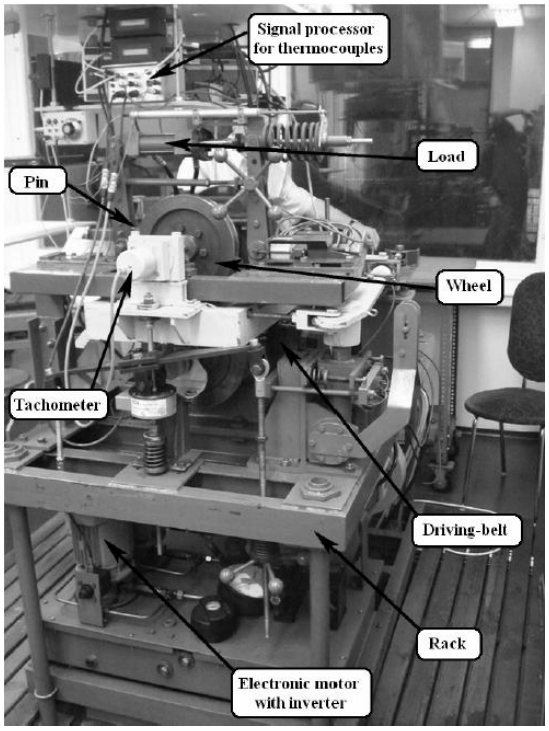

Fig. 1. General view of the testing rig

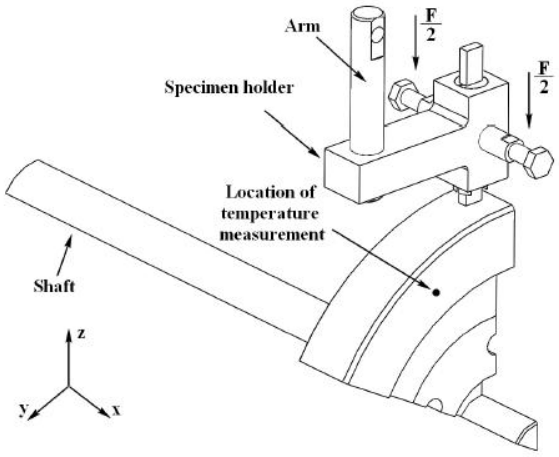

Fig. 2. Schematic description of the tested configuration

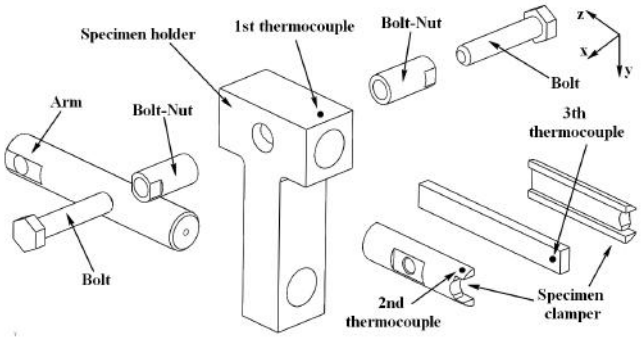

Fig. 3. Main component of the specimen holder.

The measurement started by increasing the angular velocity of the wheel to a prescribed value. Then the pin side was pushed

towards the cylindrical surface of the wheel made of steel until the intended load value was reached. During the measurement the required value was adjusted by manual interventions. The interventions can clearly be seen in the measured results. The test duration was about 800 s, which contains the uploading phase and the cool-down phase, which are always highlighted by shadowing in the resulted figures. The time history of the measured normal force is shown in Fig. 4. The figure shows the main time values, when drastical change can be observed in the force value due to the interventions mentioned.

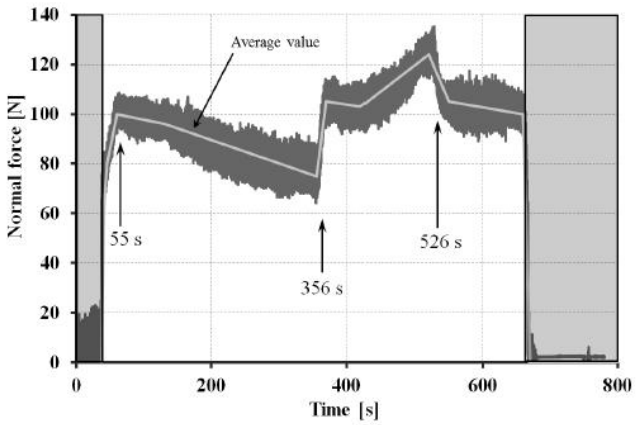

Fig. 4. Measured normal force vs. time curve and its average

The measured tangential force can not be evaluated due to the high fluctuation. The fluctuation might be the consequence of dynamical vibration of the pin like specimen. This vibration is general in steel-steel contact and generally accompanied with high-pitched voice, which was experienced during the measurements.

The temperatures measured with the thermocouples in the locations indicated in Fig. 3 can be seen in Fig. 5.

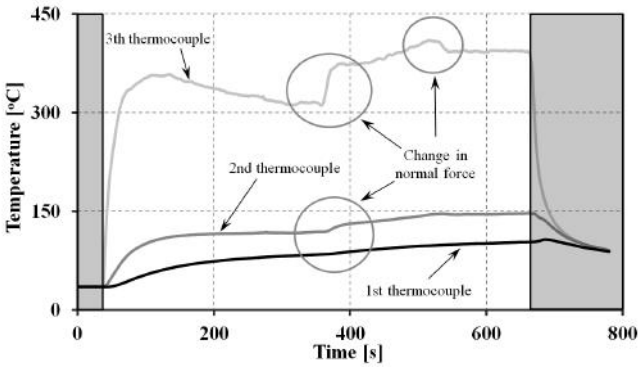

Fig. 5. Measured temperatures

It can be seen that the measured temperature near to the contact surface is about 400°C. The heat conduction is importantly reduced by the contact of the components, so the temperature at the 2^{nd} thermocouple is about 120 °C. However there is no significant difference in the time variation tendencies of the 2^{nd} and 1^{st} thermocouples temperatures. It can also be seen that the variation in temperature characteristically follows the variation in normal force value however 10-20 s time delay is present between them. The changes in the normal force (in the middle of the test) cause smaller changes in the 2^{nd} and 1^{st} measured temperatures in comparison with the 3^{rd} one. The temperature of the wheel is measured in every 201s in the spot shown in Fig. 2 by using laser temperature tester. The time of the measured temperatures is depicted in Fig. 6.

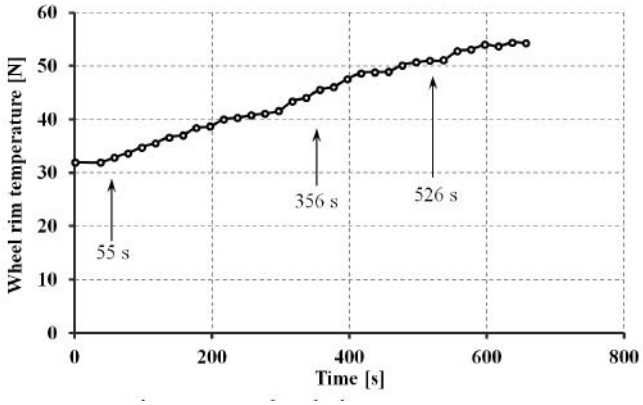

Fig. 6. Wheel rim temperature

It is also evident that the temperatures do not follow the fluctuation of normal force, as it is found on the locations of the specimen holder. However the low temperature continuously increase to 55°C which is much less than the temperatures measured in any other location.

3 FE simulation

In order to complement the measured force and temperature results finite element simulations have been carried out using commercial finite element software MSC. Marc [9]. The model takes into account the main influencing parameters like the temperature dependent material properties, the friction coefficient, and the varying contact heat transfer coefficients (this is the reciprocal of the contact resistance). The simulations partly focus on the widely accepted concept about the equality of the contact temperatures between sliding bodies, however the experiments show that the heat partition may change upon time under different thermal circumstances. Then the exact heat partition values are identified by using the test results and are validated by a moving heat source model.

3.1 Thermal model

In order to compute the temperature distribution for the tested configuration shown in Fig. 2, the construction is divided into two separate parts. The first part contains the specimen and its connecting elements while the other part includes the wheel and the driving shaft. The meshed parts can be seen in Fig. 7.

The specimen model has 80858 tetrahedron elements while the wheel model contains 80238 ones. The applied material proper-

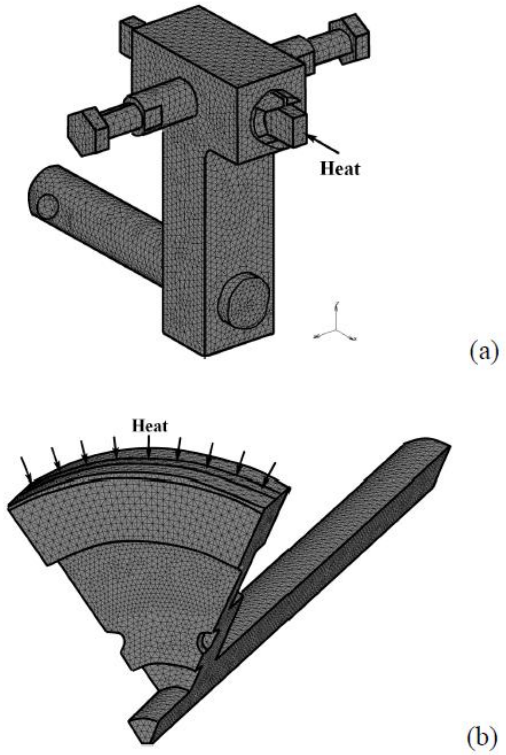

Fig. 7. Separate FE models for thermal analyzes using the pin model (a) and the wheel model (b)

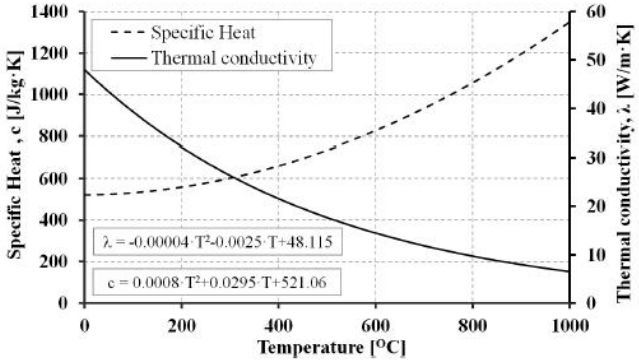

Fig. 8. Temperature dependent specific heat and thermal conductivity of the tested pin [10]

ties –identified by separate tests- can be seen in Tab. 1. The temperature dependent material properties for the specimen have been shown in separate figures according to Tab. 1.

The ambient air temperature was equal to 32°C. The heat transfer coefficient between the outer surfaces of the specimen model is represented by the widely applied 5 W/m^2·K value for air at rest. However the rotating wheel possesses higher heat transfer coefficient, which was varied according to the changing peripheral speed of the wheel. The numerical values of the applied coefficients (for part 2) are shown in Fig. 9.

The parts of the FE models are built up independently, thus it is required to define thermal (rigid) contact condition. The connection can rapidly be accomplished by the built in contact parameter called contact heat transfer coefficient. This parameter needs to be given for every contact relation separately. In our models we distinguish direct and indirect contact relations. In the case of direct connections the heat transfer is realized by steel-steel contact, which represents more continuity than the indirect connection, when the heat transfer is disturbed by air gaps which are approximately some tenth of mm. Fig. 10 represents the contact types.

Tab. 1. Applied material properties [10] **Tab. 1**

	Specimen	Wheel	Other parts
Elastic modulus [GPa]	102	200	200
Poisson ratio [-]	0.25	0.3	0.3
Density [kg/m^3]	7150	7860	7860
Thermal conductivity [W/m·K]	See Fig. 8	52	52
Specific heat [J/kg·K]	See Fig. 8	486	486
Therm. expansion coeff. [1/K]	1.3·10^{-5}	1.3·10^{-5}	1.3·10^{-5}
Initial temperature [^{o}C]	32	32	32

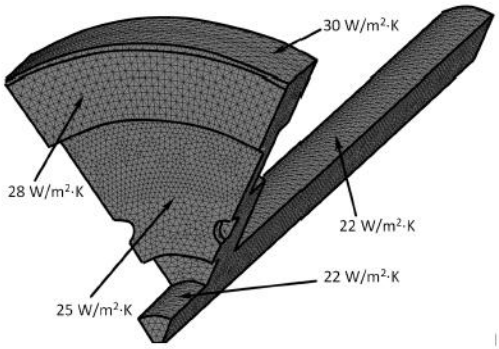

Fig. 9. Applied heat transfer coefficients

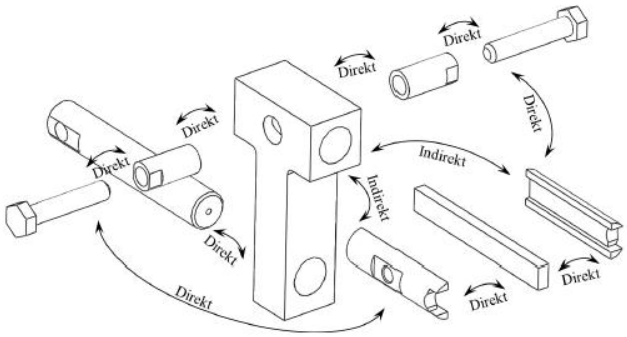

Fig. 10. Contact types for identifying the heat transfer coefficients

In the wheel model the only contact is assumed to be direct due to the clear steel-steel connection. The typical indirect contact is the heat transfer which is disturbed by an air gap between the solid partners. In our calculation the heat transfer coefficient for directs contact was examined as 5000 W/m^2, while for the indirect one as 1000 W/m^2.

The applied heat flux density has been calculated by the equation of frictional heat generation as follows:

$$q = \mu pv = \mu \frac{F}{A} v, \tag{1}$$

where q is the heat flux density, μ is the coefficient of friction realized in the sliding contact, p is the contact pressure (now uniform) and v is the sliding speed in the contact, while F represents the normal force acting between the contacting surfaces and A is the nominal surface area computed with the knowledge of the cross section of the rectangular shaped pin like specimen. The temperature dependence of the coefficient of sliding friction is shown in Fig. 11.

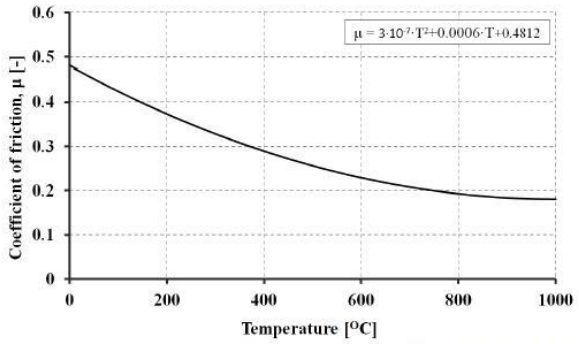

Fig. 11. Temperature dependent coefficient of friction [10]

The total heat flow generated (Q) can be computed by considering areas of the heated surfaces as

$$Q = qA = \mu F v, \tag{2}$$

In this paper authors apply the heat flux density as a thermal load. The applied value is computed by Eq. (1) but in the equation the coefficient of friction is temperature dependent (from Fig. 11) and also the normal force varies with time (according to the average value given in Fig. 4). The computed heat flux density can be seen in Fig. 12. The figure also shows the heat flux density calculated by constant coefficient of friction. Its value was $\mu = 0.38$ corresponding to the contact at $T = 200°C$ (see Fig. 11)

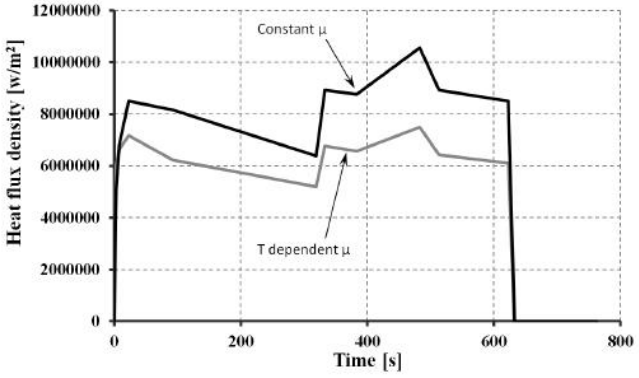

Fig. 12. Computed heat flux density

3.2 Heat partition based on contact temperature equivalence

In spite of the fact that the total heat flux can be easily computed by Eq. (1) and Eq. (2) it is essential to see that the individual heat flux values, which heat up the specimen and the contacting wheel surface cannot be directly derived from the above equations. According to the widely accepted theory, on the area of sliding contact, the condition of the equal temperatures of the partners must be fulfilled in every second, which condition determines the partition of the heat flux. Unfortunately this heat partition can be identified only by iterative computation. The heat flux partition between the contacting partners is determined by the following equations.

$$Q_{pin} = Qx \quad \text{and} \quad q_{pin} = qx, \tag{3}$$

$$Q_{wheel} = Q(1-x) \quad \text{and} \quad q_{wheel} = q\frac{a}{K}(1-x), \tag{4}$$

where value x represents the heat partition on the specimen side, a is the width of the specimen (10 mm) and K is the circumferential length of the wheel (763.4 mm). The application of Eq. (4) is correct because heat partition -entering the wheel- heats a restricted small strip of the wheel. In the current study the heat partitions are determined by transient computations. In every 50 s the x heat partition value is adjusted in order to obtain the temperature equivalence in the contact nodes. The heat partitions resulted are depicted in Fig. 13 with the resulted equilibrium temperatures by using the distributed heat source model detailed in section 3.4. It is important to see that the applied total heat flux was taken into consideration according to the curve of Fig. 12.

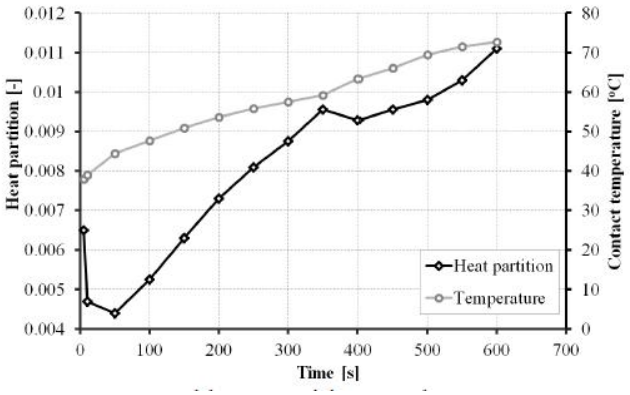

Fig. 13. Computed heat partitions and contact temperatures

It can be observed that the heat partition does not change characteristically in the time space examined. According to the computations the maximum heat flux value at the specimen side is 1.1% of the total heat flux, while the minimum is about 0.45%. The computed temperature values increase continuously and characteristic changes can not be observed. However it is essential to see that the computed surface temperature does not reach

the values of 400°C which was measured near to the contact surfaces. The difference supposedly comes from the heat partition theory. The theory states that the local contact temperature in a thin layer must be equal on both sides of the contact. However it is hard to imagine that the theory is valid when the specimen gets continuous heat load while the contacting wheel surface receive heat input periodically. The temperature inequalities are rather studied in the literature but important works [11, 12] can be found with the same observation.

3.3 Real heat partition

The heat partition is also identified by comparing the temperatures to real test results. During the calculation we used the same FE model with the time dependent heat flux density depicted in Fig. 12. However the heat partition is supposed to be constant during the whole examined time interval for ensuring the simple calculation and create transparent results. After many consecutive, iterative loops, the best agreement between the calculation and measurement is found with the x value of 10.5% which is much higher than the value determined by the classical temperature equivalence approach (1.1%). The temperature distributions are depicted in Fig. 14 for the specimen and its holder. The comparison between the measured and computed tempera-

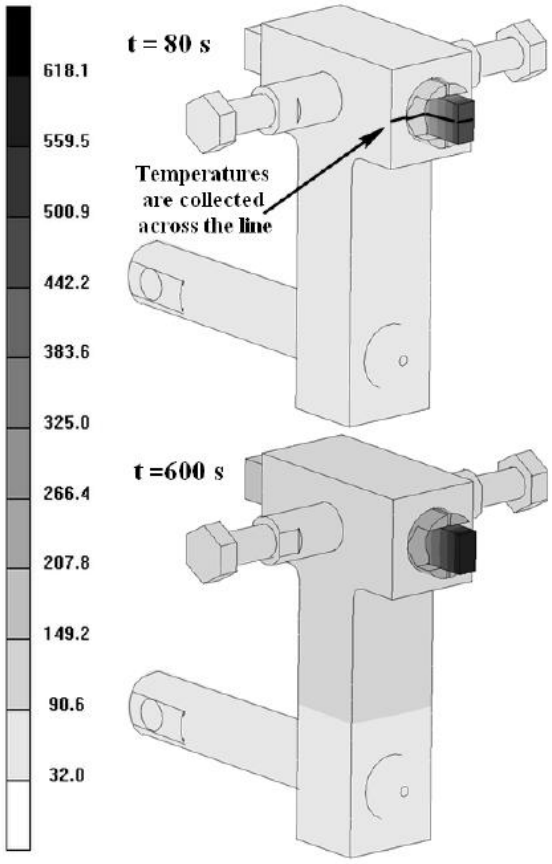

Fig. 14. Temperature distributions

tures -in the spots depicted in Fig. 3- is given in Fig. 15.

The computed results show relatively good agreement with the measured temperatures in all points. In general we establish

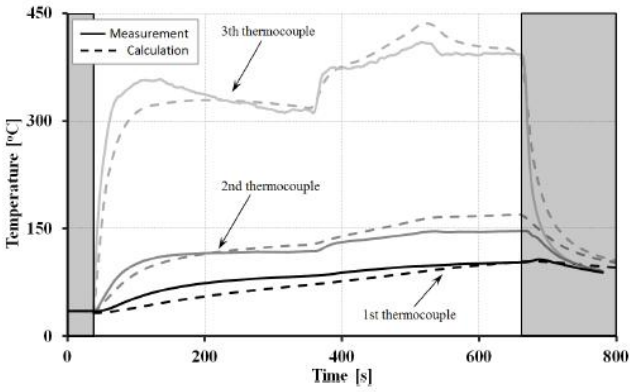

Fig. 15. Comparison of measured and computed temperatures

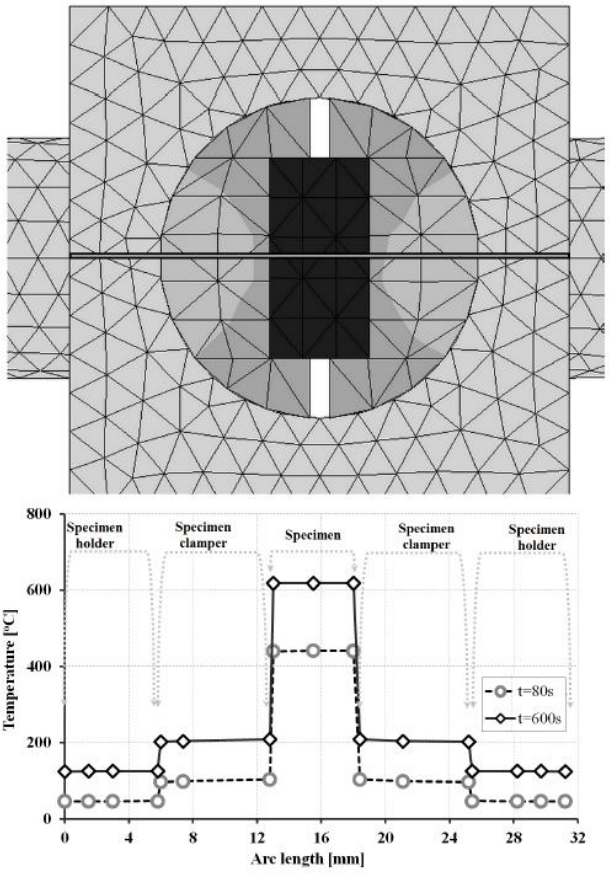

Fig. 16. Calculated temperatures across the outer surface of the specimen holder, the specimen clamper and the specimen

that the constant heat partition is not able to give realistic results for the rapid temperature changes, when the heat partition intended to suddenly modify. In order to give a more general overview on the problem, authors also depict the temperature values on the outer surface of the specimen holder, the specimen clamper and the specimen in a single diagram, which can be seen in Fig. 16. The picture clearly shows important differences on every separate part. The temperature steps are realized by the relatively large contact resistance; however it is important to note that the temperatures, depicted in Fig. 16 are collected on

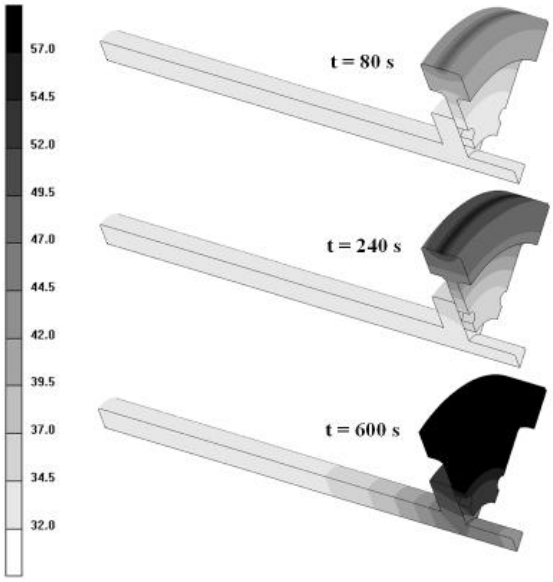

Fig. 17. Simulated temperature distributions

the surface and not on the location of thermocouples (see Fig. 3), which is the reason of the different temperatures in Fig. 15 and Fig. 16.

We also computed the wheel temperature with the same heat partition and compared the results to the measured temperatures shown in Fig. 6. The temperature distributions can be seen in Fig. 17.

The comparison of the measured and calculated wheel rim temperatures are shown in Fig. 18. The figure also gives results for the two independently identified heat partitions (10.5 % and 1.1 %). It is to be noted that the applied heat load is computed by Eq. (4).

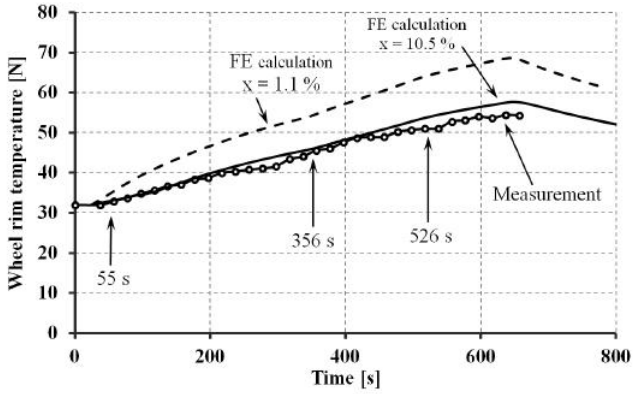

Fig. 18. Comparison of measured and computed temperatures on the wheel sliding surface (see Fig. 2)

It can be observed that the computed wheel rim temperature is in good correlation with the measured temperature in the spot shown in Fig. 2. It is also evident that the rim temperature is almost independent of/from the varying heat flux into the relatively large wheel volume. Furthermore the computation directly proves that the classical temperature equivalency based heat partition theory is not valid in the examined configuration.

3.4 Moving heat source model

In the previous models the heat source was distributed along the whole circumference of the wheel leading to the so called distributed heat source model. In the real measurement the heat source moves on the cylindrical surface of the wheel and periodically heats all the circumferential points. However the moving heat source implicates periodical, local and transient temperature processes with definite peaks. The size of the peaks compared to results received by using the distributed heat source is identified in this part in order to prove that the general behaviour of the thermal conditions can be treated with the easier distributed heat source model (if we do not intend to take into consideration the local behaviour near to the contact surface) revolution by revolution.

In order to achieve this goal the wheel model has completely modeled and meshed with 152100 hexahedral elements. The model of the wheel and the detailed view of the contact surface are shown in Fig. 19.

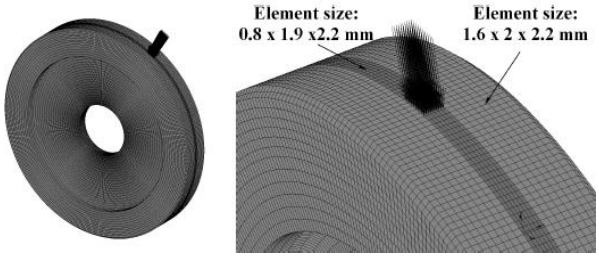

Fig. 19. Moving heat source model of the wheel and the zoomed view of the sliding contact location

Constant heat flux density, computed by Eq. (4) is used in the model by assuming the friction coefficient value of 0.38 that corresponds to the temperature of 200°C. The applied heat flux value is 8474000 W/m^2. The circumferential length of the wheel cylinder jacket has been divided into 78 surfaces, which are loaded by the heat flux after another according to the rotation speed of the wheel. The timing of the surface loading is accomplished by time tables. In order to compose the tables, firstly we need to compute the time of a complete revolution as

$$t^* = \frac{K}{v} = \frac{d\pi}{v} = \frac{2 \times 121.5 \times \pi}{11.15 \times 10^3} = 0.06846s \qquad (5)$$

The duration of the effective heat input of the heat source (due to the discrete partition of the circumferencial length) is defined by

$$t_{stand} = \frac{t^*}{78} = \frac{0.06846}{78} = 0.000877s \qquad (6)$$

where the value 78 in the denominator is the number of surfaces. The desired time step for the computation is 0.00002 s which leads to 3423 increments per complete revolutions. One example for the time table can be seen in Fig. 20.

The model contains 78 timing diagrams, which are identical with the one given in Figure 20, but are shifted $i \times xt_{stand}$(where

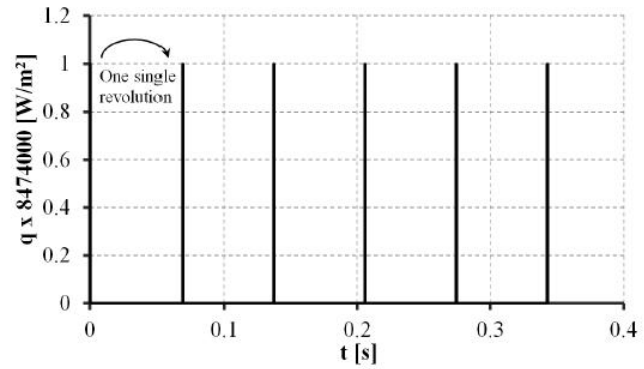

Fig. 20. Pulse like timing diagram example for the moving heat source model

i is the series number of table) with respect to the generating initial diagram.

The computation was repeated with the distributed heat source model using constant heat flux density. The comparison of the temperature distributions of the two thermal models is depicted in Fig. 21 for the first five revolutions.

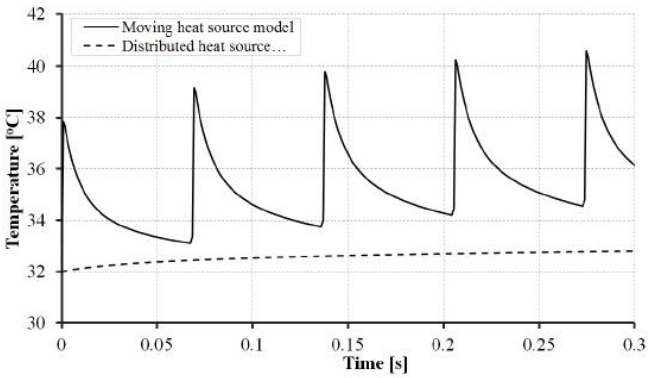

Fig. 21. Comparison of the temperature vs. time diagrams belonging to the distributed and moving heat source models

The temperature shows about 6°C variation in every single revolution and follows the law of transient characteristic of the temperature decrease. Furthermore it can be concluded that the distributed heat source model can be used instead of the more complicated moving heat source model.

4 Conclusions

The present paper introduces the small scale level thermal examination of a pin-like specimen operating on a rotating cylinder jacket. The measurement results are intended to reproduce by FE simulations using the heat partition approach. The resulted temperatures are deviating from the measured ones so the exact heat partition characteristics are computed iteratively based on the measured temperatures. The computations evidence that the classic heat partition model which considers the temperature equality on the contact surfaces cannot be used to simulate the behaviour of our specimen on cylinder jacket configuration only with inaccuracy. We suppose that one of the main reasons which cause the deviation is the high rotation speed i.e. the high relative sliding speed of the wheel surface. The high speed causes little heated volume (see Fig. 19) which change their position (move in peripheral direction) and spend a very short time under the heating interaction at a certain position. During this little time interval the applied heat flux is unable to significantly increase the wheel temperature (only 6°C from moving heat source model) which primarily penetrates into the inner part of the cold wheel and only secondly transfers to the neighbor environment. Large part of the friction generated heat (almost 90%) enters into the wheel; however it is distributed in a large volume, which causes low temperatures also near the sliding interface. On the other hand the rest of the friction induced heat warms continuously the pin, which results considerable temperature near to the interface. It is also proven that the used distributed heat source model can be used to manage the thermal problem and the results are confirmed by a moving heat source model.

References

1 **Anderson A E, Knapp R A**, *Hot spotting in automotive friction systems*, Wear **135** (1990), 319–337, DOI 10.1016/0043-1648(90)90034-8.

2 **Barber J R**, *Thermoelastic instabilities in the sliding of conforming solids*, Proc. R. Soc **A312** (1969), 381–394, DOI 10.1016/0043-1648(70)90021-9.

3 **Lee K, Barber J R**, *Frictionally excited thermoelastic instability in automotive disc brakes*, J. Tribology **115** (1993), 607–614, DOI 10.1115/1.2921683.

4 **Thuresson D**, *Stability of sliding contact –comparison of a pin and a finite element model*, Wear **261** (2006), 896–904, DOI 10.1016/j.wear.2006.01.037.

5 **Geijselaers H J M, Koning A. J. E.**, *Finite Element Analysis of Thermoelastic Instability With Intermittent Contact*, J. Tribology **122** (2000), 42–46, DOI 10.1115/1.555327.

6 **Ciavarella M, Johansson L, Afferante L, Klarbring A, Barber J R**, *Interaction of thermal contact resistance and frictional heating in thermoelastic instability*, Int. J. Solids Struct **40** (2003), 5583–5597.

7 **Vernersson T**, *Thermally induced roughness of tread-braked railway wheels, Part 1: brake rig experiments*, Wear **236** (1999), 96–105, DOI 1016/S0043-1648(99)00260-4.

8 **Vernersson T**, *Thermally induced roughness of tread-braked railway wheels, Part 2: modelling and field measurements*, Wear **236** (1999), 106–116, DOI 10.1016/S0043-1648(99)00261-6.

9 **MSC.Marc. Volume A**, *Theory and User Information*. Version 2007R1.

10 **Kretter O, Aal U A, Zobory I**, *Modellierung der Klotzbremse*, ZEV+DET Glas.Ann **118** (June 1994), no. 6.

11 **Komanduri R, Hou Z B**, *Analysis of heat partition and temperature distribution in sliding systems*, Wear **251** (2001), 925–938, DOI 10.1016/S0043-1648(01)00707-4.

12 **Kennedy T C, Plengsaard C, Harder RF**, *Transient heat partition factor for a sliding railcar wheel*, Wear **261** (2006), 932–936, DOI 10.1016/j.wear.2006.01.016.